Applied Science and Engineering Progress, Vol. 20, No. 3, 2027, 8287

Research Article

Dual-Functionalized Palm Kernel Shell Biochar as a Heterogeneous Catalyst for Glycerol Acetylation toward Biofuel Additives

Heny Dewajani*, Listiyana Candra Dewi, Asalil Mustain, Rosita Dwi Chrisnandari, and Deni Fadilah Akbar
Chemical Engineering Department, State Polytechnic of Malang, Malang, Indonesia

* Corresponding author. E-mail: heny.dewajani@polinema.ac.id DOI: 10.14416/j.asep.2026.08.013
Received: 1 May 2026; Revised: 30 June 2026; Accepted: 13 July 2026; Published online: 24 August 2026
© 2026 King Mongkut's University of Technology North Bangkok. All Rights Reserved.

Abstract
Indonesia generates abundant palm kernel shell residues with high carbon content, offering strong potential for valorization into functional materials. In this study, palm kernel shell biochar was developed as a heterogeneous catalyst through a dual-functionalization approach involving sulfonation and nickel impregnation to enhance catalytic performance in glycerol acetylation. The sulfonation and nickel impregnation steps were designed to introduce Brønsted- and Lewis-type acidic functionalities, aiming to create synergistic effects that improve reaction efficiency. Biochar was prepared via batch carbonization at 500 °C for 3 h, followed by sulfonation using concentrated sulfuric acid and subsequent nickel impregnation (5 wt%). The catalysts were characterized using SEM–EDX, BET, FTIR, and XRD analyses, confirming successful incorporation of functional groups and metal species. The sulfonated/nickel-impregnated biochar exhibited a significantly higher specific surface area (180.015 $m^2 g^{-1}$), indicating improved pore structure and accessibility of active sites. Catalytic evaluation showed that glycerol conversion increased from 43.59% for sulfonated biochar to 50.43% after nickel impregnation, suggesting a beneficial effect of combining sulfonated and nickel-modified biochar functionalities. Product analysis indicated the formation of acetylated glycerol derivatives, tentatively identified as monoacetin, diacetin, and triacetin based on GC-MS library matching. Application testing revealed that adding 7 vol% bioadditive to commercial gasoline increased the octane number from 94 to 104, reduced CO emissions from 4.46% to 2.47%, and increased CO_2 emissions from 3.50% to 5.53%, indicating improved combustion efficiency. These results demonstrate that dual-functionalized palm kernel shell biochar is a promising catalyst for glycerol valorization and biofuel additive production, offering a sustainable approach that integrates biomass utilization with enhanced fuel performance. A limitation of this study is that catalyst acidity was not directly quantified; therefore, the proposed Brønsted-type and Lewis-type acidic behavior is inferred from indirect structural, compositional, and catalytic-performance evidence.

Keywords: Biofuel additives, Dual-functionalized biochar, Glycerol acetylation, Heterogeneous catalyst, Nickel impregnation

1 Introduction

Indonesia remains one of the leading global producers of palm oil, generating more than 47 million tonnes annually and consequently producing significant quantities of biomass residues [1]. Among these residues, palm kernel shells represent a carbon-rich byproduct with high lignocellulosic content, comprising cellulose, hemicellulose, and lignin, making them an attractive precursor for developing functional carbon materials [2]. Despite their abundance, their utilization is still largely limited to low-value applications, indicating a strong opportunity for valorization into high-performance materials.

Carbon-based materials derived from lignocellulosic biomass have gained considerable attention due to their tunable pore structure, high surface area, and chemical stability. These characteristics make them suitable for applications in adsorption, energy storage, and heterogeneous catalysis [3]. However, raw biochar typically exhibits limited catalytic activity due to an insufficient number of active sites. Therefore, surface modification strategies are required to enhance both physicochemical properties and catalytic performance [3].

Applied Science and Engineering Progress, Vol. 20, No. 3, 2027, 8287

Recent literature has further emphasized the growing role of biomass-derived carbon materials and biochar in catalytic biorefinery applications, as well as the importance of pyrolysis conditions in tailoring their structure and functionality for advanced material and catalyst development [4], [5]. Among the available modification approaches, sulfonation is widely used to introduce sulfonic functional groups (–SO_3H), which are commonly associated with Brønsted-type acidity and are important for acid-catalyzed reactions such as esterification and acetylation [6]. In parallel, metal impregnation may provide additional Lewis-type acidic behavior and improve structural stability, thereby enhancing catalytic efficiency [7]. Nickel-based catalysts, in particular, have demonstrated promising activity in glycerol conversion processes due to their ability to activate reactant molecules and facilitate reaction pathways [8]. Nevertheless, the integration of both sulfonic functional groups and metal species within a single biomass-derived carbon matrix remains relatively underexplored.

Glycerol acetylation has emerged as a viable route for valorizing glycerol, a major byproduct of biodiesel production, into value-added compounds such as monoacetin, diacetin, and triacetin [9], [10]. Among these, triacetin is of particular interest as a biofuel additive because its oxygenated structure can improve combustion efficiency and increase the octane number [11], [12]. The performance of this reaction is strongly influenced by catalyst acidity, pore structure, and the accessibility of active sites, highlighting the importance of catalyst design from a chemical engineering perspective [7], [9].

Previous studies have reported various catalyst systems for glycerol acetylation, including sulfonated carbon materials, graphene-based catalysts, and metal-supported catalysts [9], [10], [13]. In addition, metal oxide catalysts functionalized with acidic groups and nickel-supported catalysts have shown the ability to enhance acetin formation and improve fuel properties [13], [14]. However, most of these studies focus on either Brønsted-type or Lewis-type behavior independently. The potential synergistic effect of combining these functionalities, particularly in biomass-derived carbon systems such as palm kernel shell biochar, has not been extensively investigated.

In this work, palm kernel shell biochar was modified through a dual-functionalization approach involving sulfonation and nickel impregnation to develop a heterogeneous catalyst with enhanced surface characteristics and catalytic performance. The prepared catalysts were systematically characterized using SEM–EDX, BET, FTIR, and XRD analyses to evaluate their physicochemical properties. Their catalytic performance was then assessed in glycerol acetylation, followed by application testing of the resulting products as bio-additives in commercial fuel. This integrated approach not only addresses biomass valorization but also provides insights into catalyst design and process performance for sustainable fuel applications. For clarity, the general acetylation reaction mechanism over sulfonated catalysts is presented in Figure 1 as background information to support the discussion of catalyst behavior.

Glycerol acetylation over solid Brønsted acid catalysts proceeds through consecutive esterification reactions, in which glycerol is sequentially converted to monoacetin, diacetin, and finally triacetin. The reaction is initiated by protonation of the carbonyl oxygen of acetic acid, followed by nucleophilic attack of the hydroxyl group of glycerol, formation of a tetrahedral intermediate, elimination of water, and regeneration of the acidic active site. This reaction pathway has been widely reported for sulfonated carbonaceous catalysts and other heterogeneous solid acids [6], [9], [15].

2 Materials and Methods

2.1 *Materials*

The materials used in this study included palm kernel shells (Ketapang, West Kalimantan, Indonesia), glycerol (99.5%), glacial acetic acid (99.8%), sulfuric acid (98%), and nickel nitrate hexahydrate, all procured from SmartLab. Additional materials included 0.1 N NaOH, phenolphthalein indicator, and deionized water.

2.2 *Methods*

The study consisted of five stages: (1) biochar preparation, (2) biochar modification, (3) catalyst characterization, (4) glycerol acetylation, and (5) evaluation of the acetylation products as additives in commercial fuel.

2.2.1 Preparation of sulfonated biochar

Palm kernel shells (1 kg) were carbonized by batch carbonization in a pyrolysis reactor at 500 °C for 3 h with a heating rate of 25 °C min^{-1} under continuous nitrogen blanketing at 1 bar, then ground and sieved through a 60-mesh screen. A schematic diagram of

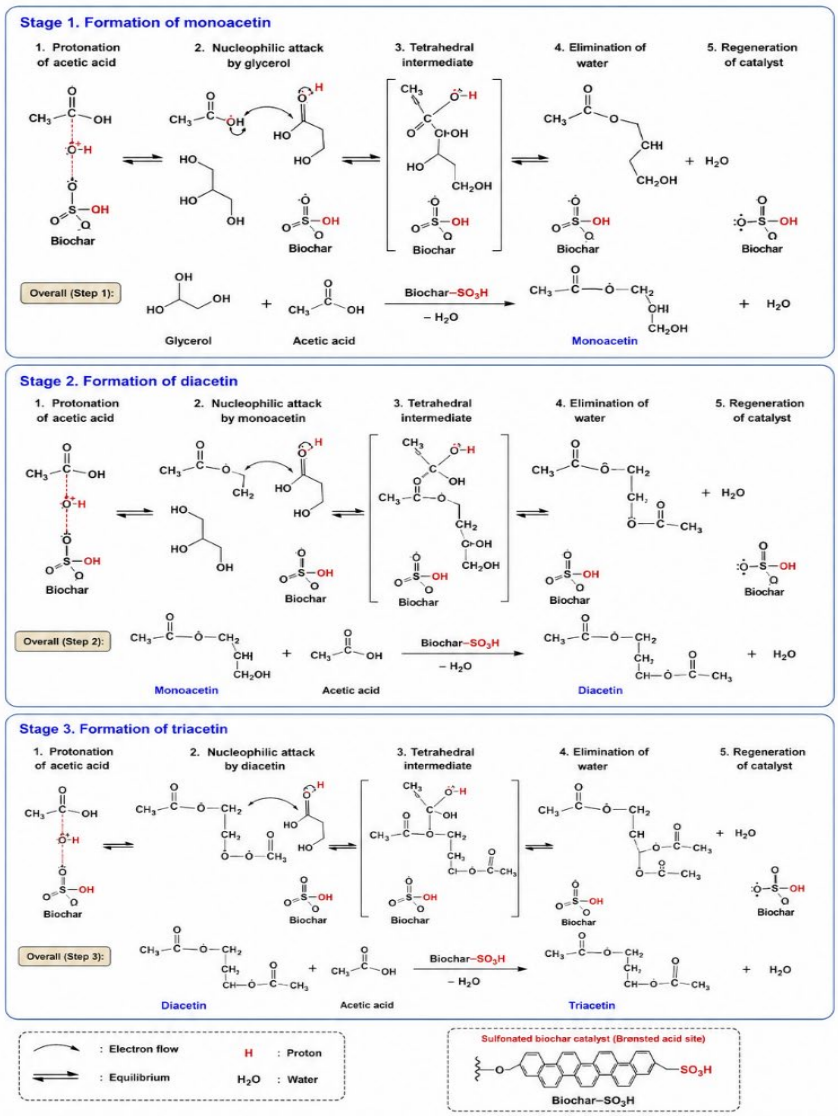

Figure 1: Proposed reaction pathway for the stepwise acetylation of glycerol with acetic acid over a sulfonated biochar catalyst (adapted from Refs. [6], [9], [15]).

the pyrolysis reactor is not included in this manuscript; however, the key operating conditions required to ensure oxygen-limited carbonization are reported here. The resulting biochar was sulfonated using 98% H_2SO_4 (biochar-to-acid ratio of 1:10, w/v) at 70 °C for 3 h. The solid was washed with deionized water to neutral pH, dried at 105 °C for 1 h, and calcined in a muffle furnace (Nabertherm L9/11 (Germany)) at 500 °C for 3 h, following the reported sulfonated carbon catalyst preparation procedure [6].

2.2.2 Preparation of sulfonated/nickel-impregnated biochar

Nickel impregnation was performed by dispersing 100 g of sulfonated biochar in an aqueous solution containing 24.68 g of $Ni(NO_3)_2 \cdot 6H_2O$ to achieve a nominal nickel loading of 5 wt%. The suspension was stirred at 85 °C for 3 h, then filtered and washed. The resulting solid was dried at 105 °C for 1 h and calcined in a Nabertherm L9/11 muffle furnace (Germany) at 500 °C for 3 h to obtain the sulfonated/nickel-impregnated biochar catalyst.

2.2.3 Characterization of catalysts

Sulfonated and sulfonated/nickel-impregnated biochar catalysts were characterized using SEM–EDX, BET, FTIR, and XRD. Proximate analysis of sulfonated biochar was conducted according to SNI 06-3730-1995 to determine moisture content, ash content, volatile matter, and fixed carbon content. Surface morphology and elemental composition were analyzed using SEM–EDX (Phenom Pharos G2 Desktop). The crystalline structure was examined by XRD (Bruker D8 Advance). Surface functional groups were identified using FTIR (Shimadzu IRSpirit-X). Specific surface area, pore characteristics, and adsorption behavior were determined by BET analysis using an Anton Paar Nova Touch LX4 instrument.

2.2.4 Glycerol acetylation

Glycerol and acetic acid (molar ratio 1:5) were added to a round-bottom flask. Sulfonated biochar or sulfonated/nickel-impregnated biochar was then added at catalyst dosages of 0, 2, 4, 6, and 8 wt%. The reaction was conducted at 100 °C for 3 h under stirring at 200 rpm.

Glycerol conversion was determined by alkalimetric titration of unreacted acetic acid. A 10 mL aliquot of the reaction mixture was taken, 3–5 drops of phenolphthalein were added, and the sample was titrated with 0.1 N NaOH to a persistent pale-pink endpoint. The volume of the titrant was used to calculate the residual acetic acid after the reaction. The acetylation product (bioadditive) was separated from residual reactants by simple distillation at 110 °C until no further acetic acid distillate was collected.

The chemical composition of the acetylation products was analyzed by gas chromatography–mass spectrometry (GC–MS) using a Shimadzu GCMS-QP2010S system equipped with an Agilent DB-5MS UI capillary column (30 m × 0.25 mm i.d., 0.25 μm film thickness). Helium was used as the carrier gas. The oven temperature was initially maintained at 70 °C for 5 min, then increased at 5 °C min^{-1} to 305 °C and held for 18 min. The injector temperature was 300 °C using split injection mode (split ratio 49:1). The mass spectrometer was operated under electron ionization (70 eV), with an ion source temperature of 250 °C, interface temperature of 305 °C, and scan acquisition over the m/z range of 28–600. The detected compounds were tentatively identified by comparison of the acquired mass spectra with the Shimadzu GCMSsolution/NIST mass spectral library.

2.2.5 Fuel blending and performance testing

Acetylation products (bioadditives) were blended with commercial gasoline to evaluate their effects on octane number and exhaust emissions. For octane testing, 1, 3, 5, and 7 vol% bioadditive was added to gasoline, and the octane number was recorded using an Oktis-2 Octane Analyzer. For emissions testing, gasoline containing 7 vol% bioadditive was operated in an internal combustion engine, and CO and CO_2 concentrations in the exhaust gas were measured using a four-gas exhaust analyzer (BrainBee AGS-688, Italy), operating on the non-dispersive infrared (NDIR) principle.

3 Results and Discussion

3.1 *Characterization of catalysts*

3.1.1 Proximate analysis of sulfonated biochar

Sulfonated biochar was analyzed using proximate analysis to determine its moisture content, ash content, volatile matter, and fixed carbon, and to evaluate its compliance with SNI 06-3730-1995 [16]. The moisture content (4%) was below the maximum limit (15%), indicating a minimal risk of pore blockage [17]. The ash content (6.67%) meets the 10% limit, indicating adequate porosity [18]. The volatile matter content (37.5%) exceeds the 25% limit, possibly due to carbonization at relatively low temperature and short duration, resulting in incomplete decomposition of non-carbon compounds [2]. The results are summarized in Table 1.

Table 1: Proximate analysis of sulfonated biochar [16].

Parameters	Sulfonated Biochar	SNI 06-3730-1995
Moisture	4.81%	< 15%
Ash	6.67%	< 10%
Volatile Matter	37.36%	< 25%
Fixed Carbon	55.82%	> 65%

3.1.2 Scanning Electron Microscopy–Energy-Dispersive X-ray Spectroscopy (SEM–EDX)

Morphological characterization and elemental composition analysis using SEM–EDX showed that modifying palm kernel shell biochar through sulfonation and nickel impregnation significantly altered the surface structure. Untreated biochar has a relatively smooth surface with limited porosity. After sulfonation, some pores appear partially covered by a layer, indicating the attachment of sulfonate groups (–SO_3H) [19]. In sulfonated/nickel-impregnated samples, the surface becomes denser and rougher, and small light-colored particles—likely nickel agglomerates—are observed. These particles can occlude some pores, indicating successful metal impregnation that may increase the number of active sites [20]. The SEM micrographs of the biochar samples are shown in Figure 2.

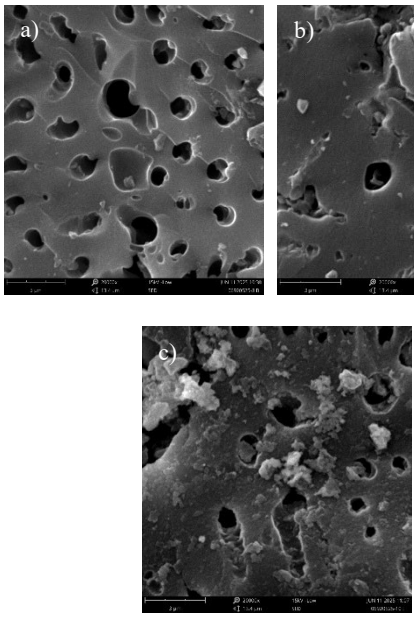

Figure 2: Scanning electron microscopy (SEM) images of (a) untreated biochar, (b) sulfonated biochar, and (c) sulfonated/nickel-impregnated biochar, acquired at 20,000× magnification.

EDX analysis further confirmed these findings by revealing carbon and oxygen as the dominant elements in all samples, together with residual Si and Al originating from the biomass. In the Ni-impregnated catalyst, the Ni content reached 17.63%, confirming the successful incorporation of nickel species. These nickel species are likely to provide Lewis acid sites on the catalyst surface, thereby contributing to its catalytic activity. Based on Table 2, EDX analysis shows that carbon and oxygen are the dominant elements in all three samples. This indicates that palm kernel shells, which are rich in cellulose (31.33%), hemicellulose (17.94%), and lignin (48.83%), have been successfully carbonized [2]. As a biomass-based material, activated carbon generally consists mainly of carbon and oxygen [21].

The Si and Al detected in small amounts in the sulfonated and sulfonated/nickel-impregnated biochar likely originated from natural minerals in palm kernel shells (e.g., silica and aluminosilicates) [17] and from ash residues carried over during sulfonation or impregnation. In the sulfonated/nickel-impregnated sample, EDX also confirmed successful impregnation, with a nickel content of approximately 17.63% after the addition of 5 wt% Ni. The N_2 adsorption–desorption isotherms of the biochar samples are shown in Figure 3.

Table 2: Mineral composition of untreated, sulfonated, and sulfonated/nickel-impregnated biochar.

Component	Weight Percentage		
	Untreated Biochar	Sulfonated Biochar	Sulfonated/Nickel-Impregnated Biochar
C	80.43%	57.26%	59.03%
O	19.57%	31.61%	22.88%
Ni	-	-	17.63%
Si	-	10.85%	0.18%
Al	-	-	0.29%
Ca	-	0.28%	-

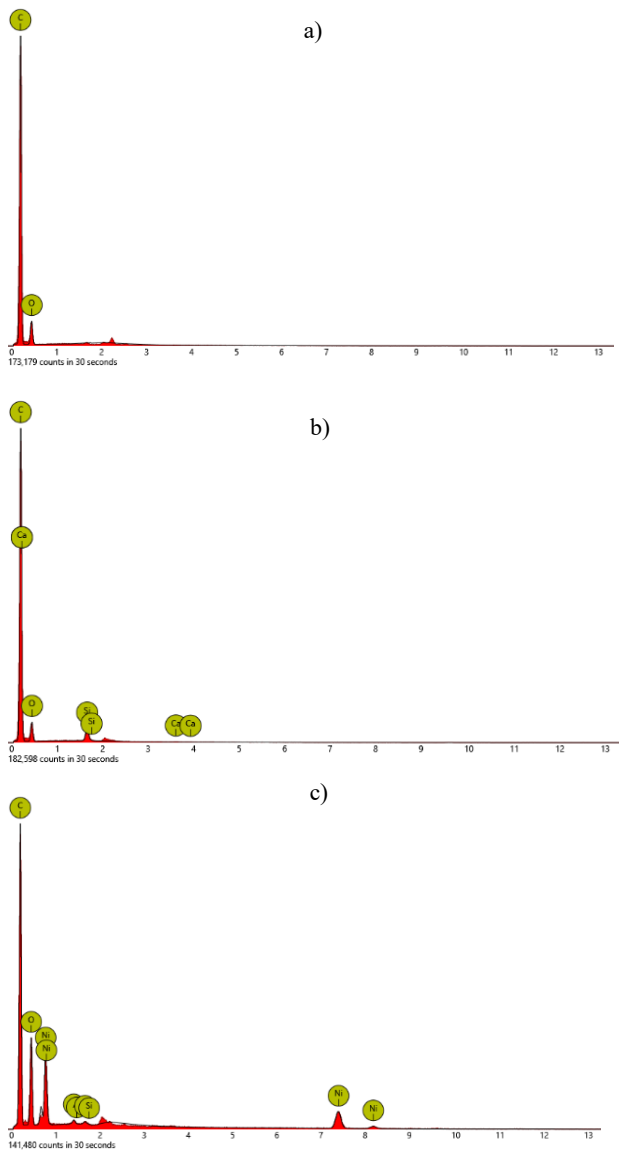

Figure 3: N_2 adsorption–desorption isotherms of untreated biochar, sulfonated biochar, and sulfonated/nickel-impregnated biochar.

3.1.3 Brunauer–emmett–teller (BET)

These morphological changes are consistent with the results of BJH and BET analyses, which show a drastic increase in specific surface area from 0.284 m^2/g in untreated biochar to 76.445 m^2/g after sulfonation, and reaching 180.015 m^2/g after nickel impregnation. This increase indicates the formation of a more open pore structure due to surface modification through oxidation and the addition of sulfonate groups (–SO_3H), consistent with activated-carbon preparation studies showing that chemical activation can enhance surface area and pore development [18]. The additional increase after nickel impregnation may be associated with the stabilizing effect of nickel on the carbon structure and its promotion of mesopore formation [22].

The total pore volume also increased, with a predominance of mesopores that facilitate the diffusion of glycerol and acetic acid molecules towards the active sites of the catalyst. The increase in pore volume after sulfonation is due to the removal of impurities and the breaking of carbon bonds [18], while impregnation provides an additional increase through changes in the internal structure and dispersion of nickel particles that prevent pore narrowing [22],[20]. The average pore diameter decreased from 15.606 nm (untreated biochar) to 3.66–3.67 nm (after sulfonation and nickel impregnation), indicating that sulfonate groups and nickel particles partially cover pore cavities while maintaining effective diffusion pathways. The increase in surface area and pore volume is expected to increase the number of accessible active sites during the acetylation reaction.

The isotherm graph in Figure 4 shows the relationship between adsorption volume (cc/g) and relative pressure (P/P_0). The adsorption–desorption isotherms exhibit characteristics of Type IV isotherms with H4-type hysteresis loops according to the IUPAC classification, indicating predominantly mesoporous structures with slit-like pores. The hysteresis reflects differences between the adsorption and desorption processes. This characteristic indicates that the material is mesoporous [23]. The corresponding pore-size distribution results obtained by the BJH method are summarized in Table 3. The hysteresis in Figure 4 resembles Type H1, which indicates mesopores with regular pore shapes. Meanwhile, Figures (b) and (c) resemble Type H4, which reflects a combination of mesopores and micropores [23].

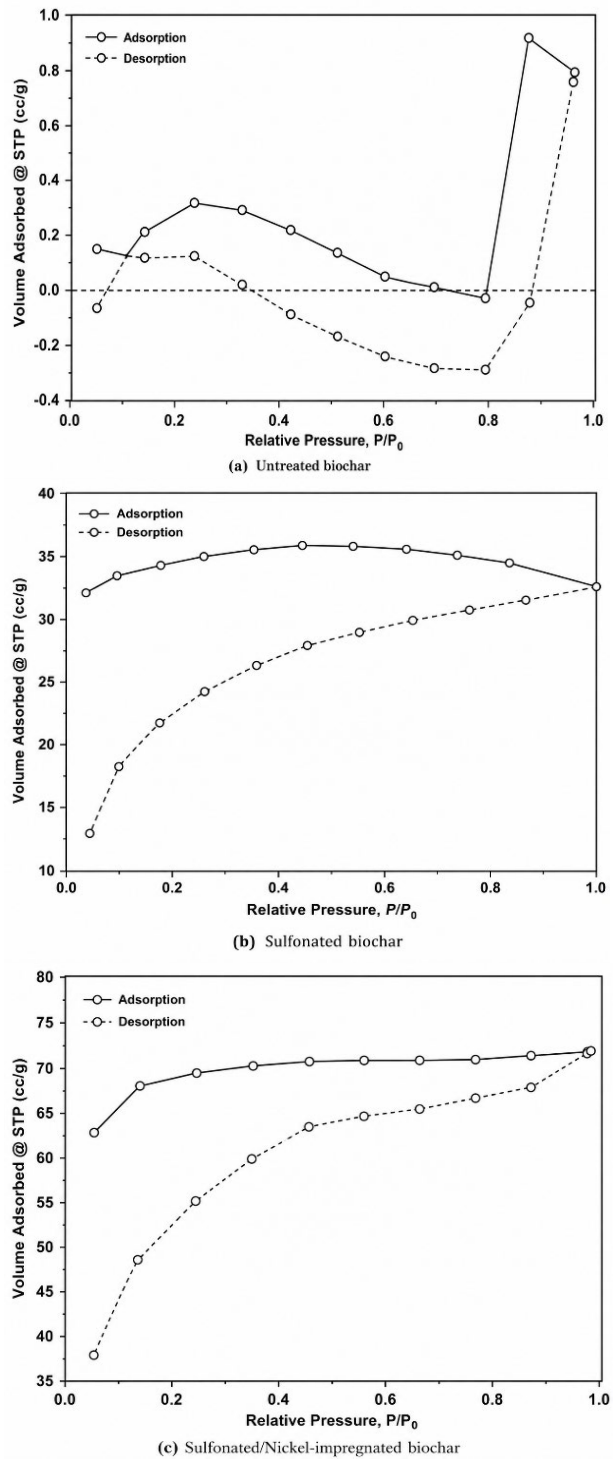

Figure 4: Nitrogen adsorption–desorption isotherms of (a) untreated biochar, (b) sulfonated biochar, and (c) sulfonated/nickel-impregnated biochar**.**

Table 3: BJH method analysis.

Characteristics	Untreated Biochar	Sulfonated Biochar	Sulfonated/Nickel-Impregnated Biochar
Surface Area (m^2/g)	0.284	76.445	180.015
Pore Distribution:			
Volume Micropore	0.00 %	0.00 %	0.00 %
Volume Mesopore	100 %	100 %	100 %
Volume Macropore	0.00 %	0.00 %	0.00 %
Total Pore Volume (cc/g)	0.002294	0.014853	0.0191561
Average Pore Diameter (nm)	15.606	3.665	3.670

3.1.4 Fourier transform infrared spectroscopy (FTIR)

Identification of functional groups by FTIR shows that untreated biochar contains aromatic groups characteristic of lignocellulose, such as aromatic C–H (754–821 cm^{-1}) and aliphatic C–H (2927 cm^{-1}) [2]. The sulfonation process enhances O–H stretching absorption at 3200–3500 cm^{-1}, indicating the presence of hydroxyl groups resulting from acid activation [24]. Although the characteristic sulfonate band (–SO_3H) at 1200–1100 cm^{-1} was not detected after calcination, this is consistent with literature reporting thermal decomposition of sulfonate groups to SO_2 at 200–300 °C [6]. In the sulfonated/nickel-impregnated catalyst, the FTIR spectrum showed no significant differences compared with the sulfonated catalyst, indicating that nickel impregnation did not substantially alter the oxygen-containing surface functionalities introduced during sulfonation. The FTIR spectra of the biochar samples are shown in Figure 5. The corresponding FTIR spectral band assignments are summarized in Table 4.

Table 4: FTIR spectral of untreated, sulfonated, and sulfonated/nickel-impregnated biochar.

Functional Groups	Wave Number		
	Untreated biochar	Sulfonated biochar	Sulfonated/nickel-impregnated biocha
C – H bending	754.17 821.68	754.17 821.68 879.54	758.02 823.60 881.47
C – H stretching	2927.94	-	-
O – H	-	3291.17	3230.59

3.1.5 X-Ray Diffraction (XRD)

XRD analysis (Figure 6) indicates that untreated and sulfonated biochar exhibit the amorphous characteristics of activated carbon at 2θ = 15–30° [21]. The broad diffraction peaks observed in both untreated and sulfonated biochar at approximately 2θ = 23° and 43° are characteristic of turbostratic (disordered) carbon and reflect the amorphous nature of the material, rather than true crystallinity. However, nickel impregnation produces new crystalline peaks at 2θ = 26.56°, 37.08°, 43.18°, 44.32°, 51.69°, 62.59°, and 76.15°, which are assignable to metallic Ni and/or NiO phases (JCPDS card No. 04-0850) [25]. These sharp peaks indicate a shift from a largely amorphous structure to a more crystalline structure, confirming successful nickel incorporation into the biochar matrix [26]. Calculations of crystallite size using the Scherrer equation show an increase

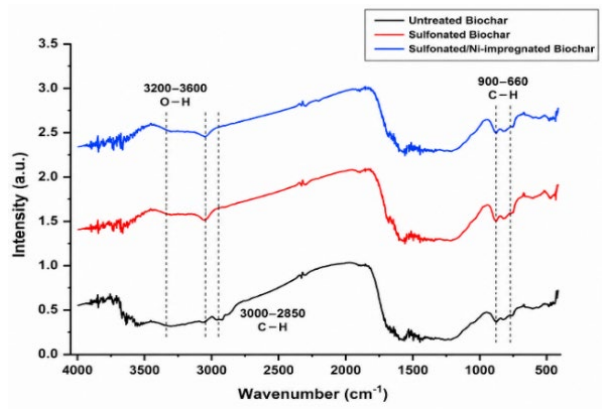

Figure 5: FTIR spectra of untreated biochar (BC), sulfonated biochar (SBC), and sulfonated/nickel-impregnated biochar (Ni-SBC) recorded in the wavenumber range 400–4000 cm^{-1}. Key absorption bands corresponding to C–H bending, O–H stretching, and aromatic C–H stretching are indicated.

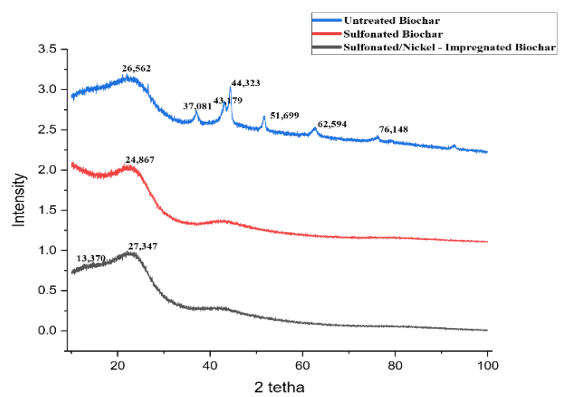

Figure 6: XRD patterns of untreated biochar, sulfonated biochar, and sulfonated/nickel-impregnated biochar**.**

Table 5: Diffraction pattern of untreated, sulfonated, and sulfonated/nickel-impregnated biochar.

Parameters	Untreated Biochar	Sulfonated Biochar	Sulfonated/Nickel-Impregnated Biochar
2θ	13.370° 27.347°	24.867°	26.562° 37.081° 43.179° 44.323° 51.699° 62.594° 76.148°
Crystallite Size (nm)	7.609	8.363	13.114

from 7.61 nm (untreated biochar) and 8.36 nm (sulfonated biochar) to 13.11 nm (sulfonated/nickel-impregnated biochar), indicating formation of a crystalline phase that may contribute to catalytic activity. The corresponding diffraction data are summarized in Table 5.

3.2 *Effect of catalyst type on reaction conversion*

As shown in Figure 7, glycerol conversion increased with increasing catalyst loading for both catalysts. In the absence of a catalyst, glycerol conversion was only 16.24%, confirming that the acetylation reaction proceeds slowly under uncatalyzed conditions. The sulfonated/Ni-impregnated catalyst consistently exhibited higher catalytic activity than the sulfonated biochar catalyst over the entire catalyst loading range. At the highest catalyst loading of 8 wt%, glycerol conversion reached 50.43%, compared with 43.59 % for the sulfonated catalyst. This enhancement can be attributed to the combined effects of a larger specific surface area, improved pore accessibility, and the presence of nickel species that may provide additional Lewis-type acidic behavior alongside the Brønsted-type acidic sites introduced by sulfonation. These synergistic effects facilitate reactant activation, enhance mass transfer, and accelerate the acetylation reaction

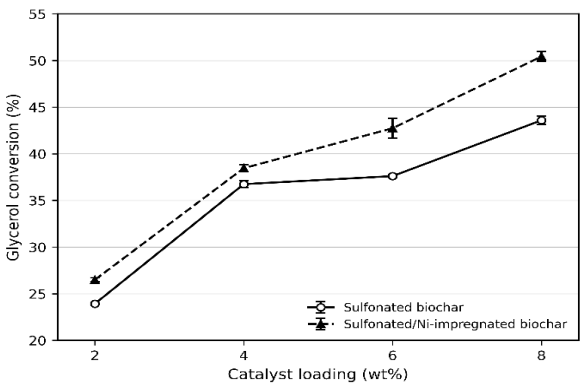

Figure 7: Effect of catalyst dosage on glycerol conversion using sulfonated biochar and sulfonated/Ni-impregnated biochar catalysts. Error bars represent the standard deviation of duplicate titration measurements (n = 2).

For sulfonated catalysts, the sulfonation process introduces sulfonic functional groups (–SO_3H) that are commonly associated with Brønsted-type acidic behavior. These surface groups may promote activation of acetic acid by increasing the electrophilicity of the carbonyl carbon and facilitating nucleophilic attack by glycerol, thereby accelerating ester formation and water production [6]. The general reaction pathway has been presented earlier in the Introduction (Figure 1) as supporting background information.

For sulfonated/nickel-impregnated catalysts, the presence of dispersed nickel species may contribute to Lewis-type acidic behavior. These nickel species may interact with the carbonyl oxygen of acetic acid, increasing the electrophilicity of the carbonyl carbon and facilitating nucleophilic attack by glycerol. As a result, ester formation may be promoted [8]. The reaction mechanism is illustrated in Figure 1.

3.3 *Effect of catalyst mass on conversion*

The acetylation reaction without a catalyst resulted in a mean glycerol conversion of 16.24 ± 0.13%. For the sulfonated biochar catalyst, the mean conversion increased with catalyst dosage from 23.93 ± 0.10% at a catalyst dosage of 2 wt% to 36.75 ± 0.35% at 4 wt%, 37.61 ± 0.17% at 6 wt%, and 43.59 ± 0.43% at 8 wt%. For the sulfonated/nickel-impregnated biochar catalyst, the corresponding mean conversions were 26.50 ± 0.23%, 38.46 ± 0.37%, 42.74 ± 1.08%, and 50.43 ± 0.52% at catalyst dosages of 2, 4, 6, and 8 wt%, respectively. Overall, conversion increased with catalyst dosage, as a higher catalyst amount provides more active sites and enhances reactant–catalyst contact. These findings are consistent with previous reports [27]-[29], which indicate that increasing catalyst mass expands the available active surface area and improves reaction efficiency. The sulfonated/nickel-impregnated catalyst exhibited the highest activity, which may be associated with the combined effect of sulfonated surface groups and nickel species, together with the larger surface area and improved pore structure. Within the dosage range investigated (0–8 wt%), glycerol conversion continued to increase without reaching a plateau, suggesting that the saturation threshold—the dosage beyond which further addition yields no additional benefit—was not reached under the present conditions and warrants investigation at higher catalyst loadings in future work. The error bars shown in Figure 7 represent one standard deviation

(±SD) calculated from duplicate titration-based measurements of glycerol conversion. The relatively small deviations indicate satisfactory repeatability of the experimental measurements and support the reliability of the observed conversion trend.

GC–MS analysis of the reaction products further supports the observed differences in catalyst performance. The reaction products obtained using the sulfonated/nickel-impregnated catalyst were tentatively identified as predominantly diacetin (50.93%) and monoacetin (38.14%), together with triacetin (10.00%), based on GC–MS library matching. In contrast, the products obtained using the sulfonated catalyst were dominated by unreacted glycerol (93.89%), with only minor amounts of monoacetin (5.01%) and diacetin (0.27%), while no triacetin was detected. The GC–MS total ion chromatograms of the acetylation products are shown in Figure 8 and summarized in Table 6. This product distribution is consistent with the higher surface area, improved pore accessibility, and enhanced surface functionality of the sulfonated/nickel-impregnated catalyst. These characteristics likely facilitated consecutive acetylation reactions, whereas the lower accessibility of active sites in the sulfonated catalyst limited further conversion of glycerol to higher acetylated products.

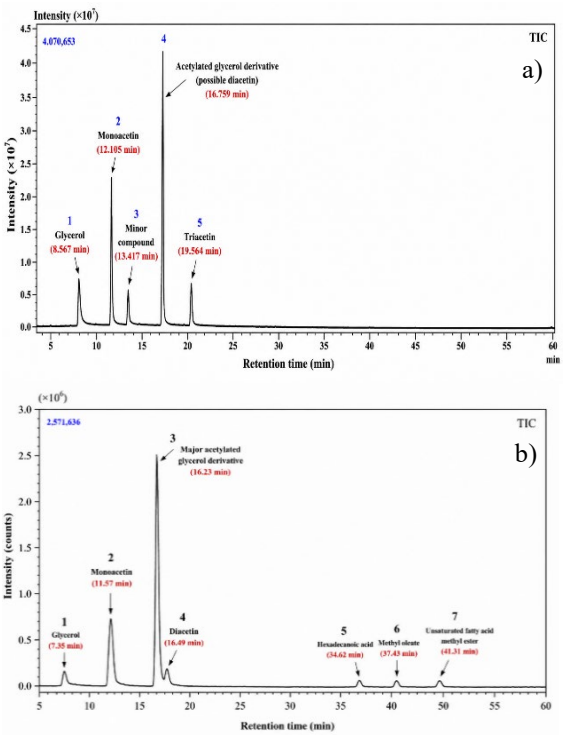

Figure 8: GC–MS total ion chromatograms of acetylation products obtained using (a) sulfonated/Ni-impregnated biochar catalyst and (b) sulfonated biochar catalyst.

Table 6: GC–MS product identification.

Catalysts	Compounds	Retention Time (min)	Area (%)
Sulfonated/Nickel-Impregnated Biochar	Glycerol	8.567	0.43
	Monoacetin	12.105	38.14
	Diacetin	16.759	50.93
	Triacetin	19.564	10.00
Sulfonated Biochar	Glycerol	7.35	94.35
	Monoacetin	11.573	5.01
	Diacetin	16.488	0.27
	Hexanoic acid	34.450	0.19
	Octadecenoic acid	37.428	0.18

3.4 *Effect of bioadditive addition on octane number*

The influence of acetylation products obtained using different catalysts is clearly reflected in their effect on the octane number of commercial gasoline. Bioadditives produced in the absence of a catalyst did not increase the octane number, whereas bioadditives produced using sulfonated catalysts increased it to 99 under selected blending conditions (Figure 9). Sulfonated/nickel-impregnated catalysts show the most significant improvement, with the highest octane number reaching 104 at a bioadditive addition of 7 vol% using a bioadditive produced with a catalyst dosage of 6 wt% of sulfonated/nickel-impregnated catalyst. This confirms that high-quality bioadditives, with optimal purity and acetyl distribution, effectively enhance fuel resistance to knocking [11], [12].

The advantages of the acetylation reaction product using sulfonated/nickel-impregnated catalysts are attributed to the properties of catalysts, including high surface area, high porosity, and the combined effect of sulfonated surface groups and nickel species, which may promote triacetin formation. As an oxygenate compound, triacetin increases the octane number by improving combustion quality and reducing the tendency for detonation, consistent with the previous findings [11], [12].

In addition to increasing the octane rating, bioadditives produced by reaction using sulfonated/nickel-impregnated catalysts also significantly improve combustion emissions (Figure 10). CO emissions decreased from 4.46% in commercial fuel without bioadditives to 2.47%, while CO_2 increased to 5.53% in fuel with a bioadditive addition of 7 vol% produced using a catalyst dosage of 6 wt% of sulfonated/nickel-impregnated catalyst, indicating improved

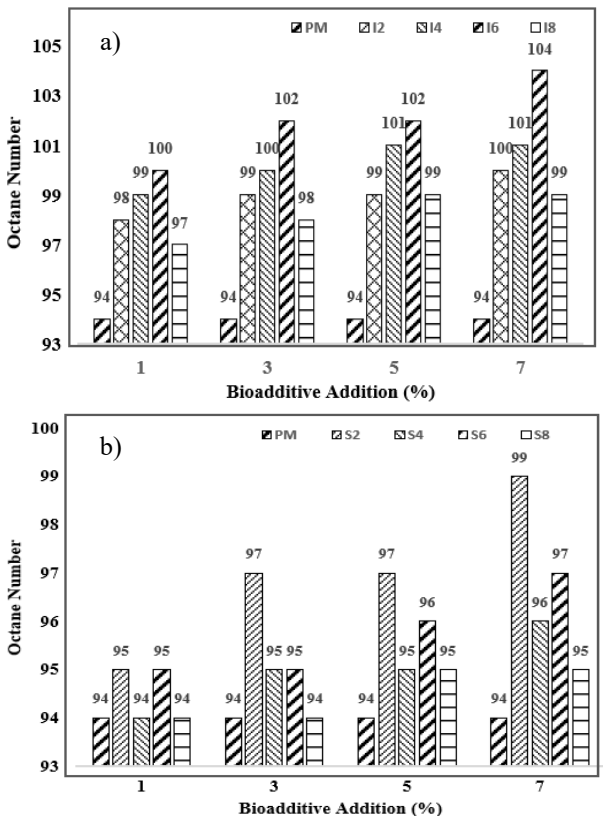

Figure 9: Comparison of fuel properties of gasoline blended with bioadditives produced using (a). sulfonated and (b). sulfonated/nickel-impregnated biochar catalysts at different catalyst dosages (Notation List: PM = without catalyst, S2 = 2 wt% catalyst dosage using sulfonated catalyst, S4 = 4 wt% catalyst dosage using sulfonated catalyst, S6 = 6 wt% catalyst dosage using sulfonated catalyst, S8 = 8 wt% catalyst dosage using sulfonated catalyst, I2 = bioadditive produced using a 2 wt% catalyst dosage of sulfonated/nickel-impregnated catalyst, I4 = bioadditive produced using a 4 wt% catalyst dosage of sulfonated/nickel-impregnated catalyst, I6 = bioadditive produced using 6 wt% catalyst dosage of sulfonated/nickel-impregnated catalyst, I8 = bioadditive produced using 8 wt% catalyst dosage of sulfonated/nickel-impregnated catalyst).

combustion efficiency. The role of triacetin as an oxygenate compound that provides additional oxygen in the fuel-air mixture improves the oxidation of CO to CO_2, as reported by [11], [12]. This trend is also consistent with broader combustion-enhancement studies using advanced fuel additives [30]. This improvement also has the potential to enhance combustion and reduce exhaust emissions, as shown in Figure 10. Overall, the best formulation was obtained with a catalyst dosage of 6 wt% of sulfonated/nickel-impregnated catalyst, resulting in a 10.64% increase in octane number and a 44.61% reduction in CO emissions. Overall, integration of the characterization and performance results indicates that sulfonation and nickel impregnation of palm kernel shell biochar simultaneously increased surface area and porosity, introduced sulfonated surface groups and nickel species, and produced a pore structure that supports reactant diffusion. These combined features led to higher glycerol conversion, a higher fraction of triacetin in the acetylation products, a significant increase in octane number, and a reduction in CO emissions in commercial fuel.

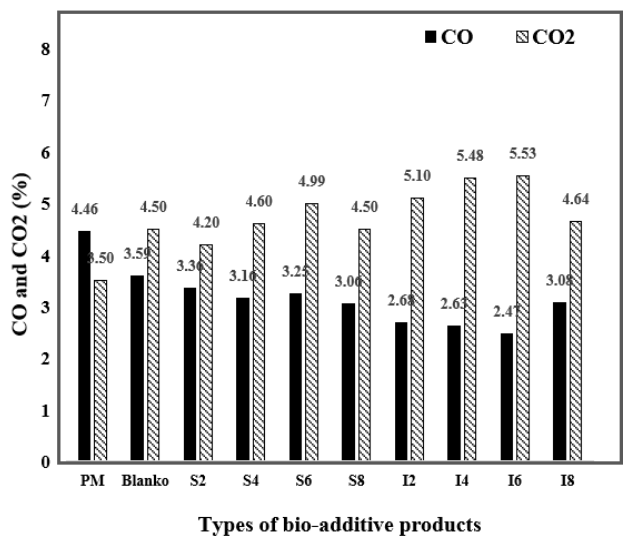

Figure 10: Comparison of exhaust gas emissions of gasoline blended with 7 vol% bioadditives produced using (a). sulfonated and (b). sulfonated/nickel-impregnated biochar catalysts at different catalyst dosages. **(**Notation List: PM = without additive, Blank = additive without catalyst, S2 = bioadditive produced using 2 wt% catalyst dosage of sulfonated catalyst, S4 = bioadditive produced using 4 wt% catalyst dosage of sulfonated catalyst, S6 = bioadditive produced using 6 wt% catalyst dosage of sulfonated catalyst, S8 = bioadditive produced using 8 wt% catalyst dosage of sulfonated catalyst, I2 = bioadditive produced using a 2 wt% catalyst dosage of sulfonated/nickel-impregnated catalyst, I4 = bioadditive produced using a 4 wt% catalyst dosage of sulfonated/nickel-impregnated catalyst, I6 = bioadditive produced using a 6 wt% catalyst dosage of sulfonated/nickel-impregnated catalyst, I8 = bioadditive produced using 8 wt% catalyst dosage of sulfonated/nickel-impregnated catalyst**).**

4 Conclusions

Palm kernel shell biochar was successfully engineered into a dual-functional heterogeneous catalyst via sulfonation and nickel impregnation, introducing sulfonated surface groups and nickel species while enhancing surface properties. This combination produced a beneficial effect, increasing glycerol conversion from 16.24% (no catalyst) to 50.43% for the sulfonated/nickel-impregnated catalyst. Catalyst dosage further influenced performance, with a catalyst dosage of 6 wt% yielding optimal results. The resulting bioadditive improved fuel quality by increasing the octane number by 10.64% and reducing CO emissions by 44.61%, indicating enhanced combustion efficiency. Overall, this work demonstrates a clear structure–property–performance relationship and highlights the potential of biomass-derived dual-functional catalysts for sustainable glycerol valorization and biofuel applications. A limitation of this study is that catalyst acidity was not directly quantified; therefore, the proposed Brønsted-type and Lewis-type acidic behavior is inferred from indirect structural, compositional, and catalytic-performance evidence. Future work should include direct acidity measurements using NH_3-TPD or pyridine-FTIR to quantitatively distinguish Brønsted and Lewis acid sites and to further validate the proposed catalytic mechanism.

Acknowledgments

The authors would like to thank the Department of Chemical Engineering at Malang State Polytechnic for providing laboratory facilities and the Smart Green Energy Research Group for supporting this research.

Author Contributions

H.D.: conceptualization, investigation, review and editing; L.C.D.: investigation, methodology, writing—original draft; A.M.: research design, data analysis; H.D., R.D.C., and D.F.A.: conceptualization, data curation, writing—review and editing, funding acquisition, and project administration. All authors have read and agreed to the published version of the manuscript.

Conflicts of Interest

The authors declare no conflict of interest.

Declaration of generative AI and AI-assisted technologies in the writing process

The authors have not utilised any generative AI tool for any assistance in the writing process.

References

[1] Badan Pusat Statistik, *Statistik Tanaman Perkebunan Tahunan Indonesia 2024 (Kelapa Sawit, Kopi, Kakao, Karet, Teh, dan Komoditas Perkebunan Unggulan)*. Indonesia: Badan Pusat Statistik, 2024.

[2] T. E. Awoh, J. Kiplagat, S. Kimutai, and A. C. Mecha, "Current trends in palm oil waste management: A comparative review of Cameroon and Malaysia," *Heliyon*, vol. 9, no. 11, Art. no. e21410, 2023, doi: 10.1016/j.heliyon.2023.e21410.

[3] R. K. Mishra, B. Singh, and B. Acharya, "A comprehensive review on activated carbon from pyrolysis of lignocellulosic biomass: An application for energy and the environment," *Carbon Resources Conversion*, vol. 7, no. 4, Art. no. 100228, 2024, doi: 10.1016/j.crcon.2024.100228.

[4] D. Hantoko, "Biomass pyrolysis: A comprehensive review of production methods, derived products, and sustainable applications in advanced materials," *Applied Science and Engineering Progress*, vol. 18, no. 2, Art. no. 7645, 2025, doi: 10.14416/j.asep.2024.11.009.

[5] Y. X. Seow, Y. H. Tan, J. Kansedo, I. S. Tan, B. L. F. Chin, N. M. Mubarak, M. N. B. Mohiddin, P. N. Y. Yek, Y. S. Chan, and M. O. Abdullah, "Pyrolysis assessment of palm kernel shell waste valorization to sulfonated magnetic biochar from techno-economic and energy perspectives," *Discover Applied Sciences*, vol. 6, Art. no. 398, 2024, doi: 10.1007/s42452-024-06079-7.

[6] L. J. Konwar, P. Mäki-Arvela, and J.-P. Mikkola, "SO_3H-containing functional carbon materials: Synthesis, structure, and acid catalysis," *Chemical Reviews*, vol. 119, no. 22, pp. 11576–11630, 2019, doi: 10.1021/acs.chemrev.9b00199.

[7] J. Keogh, P. Inrirai, N. Artioli, and H. Manyar, "Nanostructured solid/liquid acid catalysts for glycerol esterification: The key to convert liability into assets," *Nanomaterials*, vol. 14, no. 7, Art. no. 615, 2024, doi: 10.3390/nano14070615.

[8] P. Ounsuk, S. Triampitak, J. Leetrakul, K. Sudsakorn, A. Seubsai, C. Prapainainar, and P. Prapainainar, "Catalyst screening and optimization condition of green solvent for BHD production using Ni-based catalysts," *Applied Science and Engineering Progress*, vol. 17, no. 3, Art. no. 7352, 2024, doi: 10.14416/j.asep.2024.03.002.

[9] U. I. Nda-Umar, I. Ramli, E. N. Muhamad, N. Azri, and Y. H. Taufiq-Yap, "Optimization and characterization of mesoporous sulfonated carbon catalyst and its application in modeling and optimization of acetin production," *Molecules*, vol. 25, no. 22, Art. no. 5221, 2020, doi: 10.3390/molecules25225221.

[10] M. R. Ika, N. Ravina, P. Herry, and H. Nur, "Performances of carbon-based catalysts for glycerol acetylation," in *Proc. 8th Int. Conf. Engineering, Technology, and Industrial Application*, Surakarta, Indonesia, Dec. 15–16, 2021.

[11] M. Tabatabaei *et al*., "Environmental impact assessment of the mechanical shaft work produced in a diesel engine running on diesel/biodiesel blends containing glycerol-derived triacetin," *Journal of Cleaner Production*, vol. 223, pp. 466–486, 2019, doi: 10.1016/j.jclepro.2019.03.106.

[12] T. Kalyani, L. S. V. Prasad, and A. Kolakoti, "Effect of triacetin as an oxygenated additive in algae biodiesel fuelled CI engine combustion, performance, and exhaust emission analysis," *Fuel*, vol. 338, Art. no. 127366, 2023, doi: 10.1016/j.fuel.2022.127366.

[13] H. Dewajani, A. Chumaidi, A. S. Suryandari, E. N. Dewi, and M. H. Ahsan, "Characterization and preparation of Ni/γ-Al_2O_3 catalyst for acetylation of glycerol in a fixed bed reactor applied as an octane booster for commercial fuels," *Jurnal Bahan Alam Terbarukan*, vol. 10, no. 2, pp. 60–68, 2021.

[14] H. Dewajani, W. Zamrudy, H. Saroso, S. Paramarta, and W. Mulya, "Conversion of crude glycerol from by-product biodiesel into bio-additive of fuel through acetylation reaction based on modified zeolite catalyst," *Alchemy: Journal of Chemistry*, vol. 7, no. 2, p. 46, 2019.

[15] A. P. da Luz Corrêa, P. M. M. da Silva, M. A. Gonçalves, R. R. C. Bastos, G. N. da Rocha Filho, and L. R. V. da Conceição, "Study of the activity and stability of sulfonated carbon catalyst from agroindustrial waste in biodiesel production: Influence of pyrolysis temperature on functionalization," *Arabian Journal of Chemistry*, vol. 16, no. 8, Art. no. 104964, 2023.

[16] Badan Standardisasi Nasional, *Standar Nasional Indonesia Arang Aktif Teknis*, SNI 06-3730-1995. Jakarta, Indonesia: Badan Standardisasi Nasional, 1995, pp. 1–21.

[17] O. M. Ikumapayi and E. T. Akinlabi, "Composition, characteristics and socio-economic benefits of palm kernel shell exploitation-An overview," *Journal of Environmental Science and Technology*, vol. 11, no. 5, pp. 220–232, 2018.

[18] R. Chen, L. Li, Z. Liu, M. Lu, C. Wang, H. Li, W. Ma, and S. Wang, "Preparation and characterization of activated carbons from tobacco stem by chemical activation," *Journal of the Air and Waste Management Association*, vol. 67, no. 6, pp. 713–724, 2017, doi: 10.1080/10962247.2017.1280560.

[19] A. S. Suryandari, T. Nurtono, W. Widiyastuti, and H. Setyawan, "Hydrophobic modification of sulfonated carbon aerogels from coir fibers to enhance their catalytic performance for esterification," *ACS Omega*, vol. 8, no. 30, pp. 27139–27145, 2023.

[20] M. M. Marcelino, G. A. Leeke, G. Jiang, J. A. Onwudili, C. T. Alves, A. L. F. de Sousa, D. M. de Santana, F. A. Torres, S. A. B. Vieira de Melo, and E. A. Torres, "Effect of nickel nanocatalyst loading on supercritical water gasification of coconut shell," *Energies*, vol. 17, no. 4, Art. no. 872, 2024, doi: 10.3390/en17040872.

[21] M. Dizbay-Onat, "Evaluation of physical adsorption properties of the activated carbon layers used in commercial face-mask inserts," *Engineering*, vol. 4, no. 1, pp. 434–443, 2023, doi: 10.3390/eng4010026.

[22] H.-S. Jeong and B.-J. Kim, "Effects of nickel impregnation on the catalytic removal of nitric oxide by polyimide-based activated carbon fibers," *Nanomaterials*, vol. 13, no. 16, Art. no. 2297, 2023, doi: 10.3390/nano13162297.

[23] M. Thommes, K. Kaneko, A. V. Neimark, J. P. Olivier, F. Rodriguez-Reinoso, J. Rouquerol, and K. S. W. Sing, "Physisorption of gases, with special reference to the evaluation of surface area and pore size distribution (IUPAC Technical Report)," *Pure and Applied Chemistry*, vol. 87, no. 9–10, pp. 1051–1069, 2015.

[24] G. Fu, Z. Wang, Y. Zhang, Z. Huang, J. Liu, J. Zhou, and K. Cen, "Effect of raw material sources

on activated carbon catalytic activity for HI decomposition in the sulfur-iodine thermochemical cycle for hydrogen production," *International Journal of Hydrogen Energy*, vol. 41, no. 19, pp. 7854–7860, 2016, doi: 10.1016/j.ijhydene.2015.12.212.

[25] A. Allwar, N. Indriyani, R. Maulina, and F. Rahmawati, "Hydrocracking optimization of palm oil over $NiMoO_4$/activated carbon catalyst to produce biogasoline and kerosine," *Open Chemistry*, vol. 20, no. 1, pp. 1643–1652, 2022, doi: 10.1515/chem-2022-0270.

[26] P. Maneechakr and S. Karnjanakom, "Improving the bio-oil quality via effective pyrolysis/deoxygenation of palm kernel cake over a metal (Cu, Ni, or Fe)-doped carbon catalyst," *ACS Omega*, vol. 6, no. 30, pp. 20006–20014, 2021 , doi: 10.1021/acsomega.1c02999.

[27] S. Ammaji, G. S. Rao, and K. V. R. Chary, "Acetalization of glycerol with acetone over various metal-modified SBA-15 catalysts," *Applied Petrochemical Research*, vol. 8, no. 2, pp. 107–118, 2018, doi: 10.1007/s13203-018-0197-6.

[28] K. Jagadeeswaraiah, M. Malyaadri, and K. D. Reddy, "Synthesis of glycerol acetins as fuel additives: Acetylation of glycerol with SnTPA catalyst," *Journal of Chemical Sciences*, vol. 137, Art. no. 20, 2025, doi: 10.1007/s12039-025-02359-w.

[29] G. D. Yadav and S. O. Katole, "Synthesis of green bioadditives via esterification of glycerol with acetic acid catalysed by modified heteropolyacid on clay support," *Journal of the Indian Chemical Society*, vol. 102, Art. no. 101623, 2025 , doi: 10.1016/j.jics.2025.101623.

[30] M. Elkelawy, M. M. Sayed, and A. A. Mohamed, "Sustainable combustion enhancement in CI engines using advanced fuel additives," *Pharos Engineering Science Journal*, vol. 2, no. 2, pp. 309–318, 2025, doi: 10.21608/pesj.2025.389975.1033.